Trans. Phenom. Nano Micro Scales, 6(Special):20-28
DOI: 10.22111/tpnms.2018.23878.1142

ORIGINAL RESEARCH PAPER

Numerical investigation of ferrohydrodynamic (FHD) effect on forced convection of cross-corrugated triangular channels

Arash. Mahboubidoust [1,*]***, Amirhosein. Ghasemi*** [1]***, Abas. Ramiar*** [1]***, Pouyan. Vatani*** [2]

[1]*Department of Mechanical Engineering, Babol Noshirvani University of Technology, Babol, Iran*
[2]*Department of Mechanical Engineering, Sharif University of Technology, Tehran, Iran*

Received 6 February 2018; revised 10 March 2018; accepted 21 April 2018; available online 6 May 2018

ABSTRACT: Cross-corrugated triangular channels increase heat transfer in heat exchangers. The mixing effect increases the heat transfer coefficient at the surfaces. In this study, the fluid flow and heat transfer in a triangular corrugated channel are modeled under two constant heat fluxes and different Reynolds numbers. In order to validate, k-ω turbulence model is used. Also, the effect of magnetic field is investigated in different locations of the channel and the channel entrance area is shown as the optimal area for application of the magnetic field both in terms of heat transfer coefficient and friction coefficient. It is also observed that the Nusselt number always increases with Reynolds increase, but the friction coefficient only increases when the magnetic field is positioned at the entrance area of the channel with the Reynolds increase and decreases in other cases. The presented results can be helpful for improving the performance of plate heat exchangers..

KEYWORDS: *Convection heat transfer; Cross-corrugated triangular channel; Magnetic field; Nusselt number; OpenFOAM*

INTRODUCTION

Investigating forced convection is one of the most important issues discussed about the channels. Forced heat transfer has many applications in industry, such as heat exchangers, boilers, solar collectors, reactors, micro heat exchangers, electronic coolers and catalytic converters. Because of the many applications of heat exchangers in the industry, efforts have been made to provide a way to increase heat transfer.

Although with improvements in technology, heat exchangers are being built better with higher quality materials, but researches on the fluid type and the shape of the heat exchangers have improved heat transfer. Increasing heat transfer methods consists of corrugating heat exchanger wall, using nanoparticles, and applying magnetic field on the fluid. Also, to increase the heat transfer, it is possible to add particles with high thermal conductivity coefficient in nanoscale. The fluid containing these suspended particles is referred to as Nano-fluid.

As mentioned, one of the methods in order to increase heat transfer is corrugating the walls. The production of corrugated walls is easy which increases the mechanical strength of the plates, and also decreases the heat exchangers volume size as it increases heat transfer.

The increase in heat transfer in these plates is due to increased turbulence and flow mixing due to corrugation of the plates.

*Corresponding Author Email: *arashmd538 @gmail.com*
Tel.: +989371670126; Note. This manuscript was submitted on *February* 6, 2018; approved on *March* 10, 2018; published online *May 6, 2018*.

Sawyers et al. [1] investigated the heat transfer in a corrugated channel in three-dimension with a laminar flow by combining analytic and numerical methods. Their work is performed in low Reynolds numbers and only for a laminar flow. Zhang [2] investigated heat transfer and fluid flow in a corrugated path and compared its data with existing experimental values and concluded that the k-w model is the best model to investigate the flow in this conditions. In a flow with high Reynolds number, generated secondary flow has the most effect in momentum transfer. Naphon [3] investigated the fluid flow and heat transfer in several types of channels with different geometries in two-dimension, and showed the increased heat transfer in the corrugated channel as well as the sharp edge effect of the bumps in heat transfer in such channels. Zhang and Chen [4] examined the airflow in a corrugated heat exchanger under the constant heat flux boundary condition. They used the LKW method to solve the equations, and concluded that only the LKW model is consistent with experimental values, and that for the Reynolds numbers up to 1000, laminar model is acceptable, and the standard k-ε model is only applicable for Reynolds numbers above 5000. Yin and Yang [5] focused on the fluid flow and heat transfer in a sinusoidal corrugated channel with a constant temperature boundary condition in low Reynolds numbers, in which the effects of the channel surface spacing from each other, the roughness of the bumps and the mass flow rate of the fluid on the fluid flow and heat transfer is investigated. Ramiar et al. [6] investigated the effects of the presence of nanoparticles in fluid on the heat

Nomenclature

			Greek Symbols
A	Area, m^2	ρ	Density, kg m^{-3}
c_p	specific heat of air, kJ kg^{-1} K^{-1}	α	Thermal diffusivity, m^2s^{-1}
D_h	Hydraulic diameter of the channel, m	ν	kinematic viscosity, m^2s^{-1}
E_p	heating power, kW	μ	molecular viscosity, Nsm^{-2}
f	friction factor	τ	shear stress, Nm^{-2}
h	convective heat transfer coefficient, $Wm^{-2}K^{-1}$	ω	specific dissipation rate, s^{-1}
k	turbulent kinetic energy, m^2/s^2	λ	heat conductivity, $Wm^{-1}K^{-1}$
L	Length, m		
$\dot{m}_v$	mass flow rate, kg/s		**Superscripts**
P	Pressure,Pa	*	dimensionless
q”	Heat flux, (W/m^2)	'	fluctuation
T	Temperature, K		
u, v, w	Velocities, ms^{-1}		**Subscripts**
x, y, z	Coordinates, m	i	inlet
Nu	Nusselt number	o	outlet
Re	Reynolds number, U_iD_h/ν	t	Turbulent
		w	wall

transfer of a microchannel in two dimensional and in a laminar flow, and concluded that the higher the thermal capacity of the nanoparticles, the higher the heat transfer value would be. Nourani and Salmanpour [7] investigated fluid flow and heat transfer in a corrugated channel and also compared the results with the values for a straight channel. The results showed that with increase of Reynolds number, the Nusselt number increases. Also, the sharp edge effect of bumps and their number on heat transfer is investigated and it is shown that with increasing the number of bumps, heat transfer increases. In that paper, the flow is studied only in two-dimensional form in a limited range of Reynolds numbers. Al-Jabair [8] investigated the flow in a three-dimensional pattern in a channel with OpenFOAM software with different turbulence models, and showed the advantages and disadvantages of each model. Ramgadia et al. [9] examined the effect of changing Reynolds number on fluid flow and heat transfer in a two-dimensional model, and concluded that for a steady state flow, the heat transfer rate is low, but in an un steady flow with increase in the mixing between the central flow and the flow near the wall, heat transfer is increased. Midhun et. al. [10] investigated the heat transfer in different two-dimensional channels using Open-FOAM software, and determined a critical point for each channel, and concluded that the corrugated channel is the best type of canal in terms of heat transfer. Ramgadia et al. [11] also focused on calculating fully developed flow heat transfer and flow in three dimensions, observing that the friction coefficient is independent of the Reynolds number, but the Nusselt number depends on changes of Reynolds number. Benchabi and Lanani [12] investigated the flow and heat transfer in two and three dimension. They examined the effects of the Reynolds number and the protrusions' angle and the ratio of sizes on the Nusselt number and the friction coefficient, and concluded that with increasing Reynolds number, Nusselt number increases and the coefficient of friction decreases. Deylmai et al. [13] investigated the frictional pressure drop and the performance of corrugated channels for different Reynolds number ranges. It was also concluded that the turbulence model that matches the experimental values is the RNG k-ε model. Khoshvaght et. al. [14] investigated the heat transfer and flow characteristics in a two-dimensional corrugated channel using nano-fluid and examined the effects of channel height, wavelength, wave amplitude, and phase change in different Reynolds numbers and different volumes fraction of nanoparticles and determined that the channel height and wave amplitude have the greatest effect on the Nusselt number and friction coefficient. Ahmed et al. [15] studied the slow movement of Al_2O_3 nano-fluid in a sinusoidal corrugated channel for different phases of a sinusoidal wave function, and concluded that the best performance occurs to zero-degree phase and the Nusselt number increases by increasing the Reynolds number. In this paper, the flow is investigated in low Reynolds numbers and finite range of angles. Also, Ahmed et al. [16] investigated the increase in heat transfer and pressure drop of SiO_2 nano-fluid in different channels experimentally and numerically, and showed that with increasing the volumetric fraction of nanoparticles, the Nusselt number and heat transfer as well as the amount of pressure drop increase. Mirzaei et al. [17] studied the flow in a three-dimensional corrugated channel in two different Prandtl and Reynolds numbers and concluded that the changes of thickness of the thermal boundary layer was more effective than the turbulence variation on the local Nusselt number. Naghibi et al. [18] investigated the effects of the ratio of corrugated channel height, wavelength, as well as Reynolds number and volume fraction of nanoparticles on fluid flow, and concluded that with increasing Reynolds number, wavelengths of the wall and volume fraction of the

nanoparticles, the Nusselt value decreases. Gao et al. [19] investigated a three-dimensional corrugated channel by varying the channel aspect ratio numerically and showed that the bubbles separation flow and streamlines near the wall, increase with increasing wall wave amplitude and compared with the straight wall, the corrugated wall causes increased pressure, reduced friction and increased drag coefficient. Li et al. [20] obtained heat and mass transfer in a corrugated channel heat exchanger for air under different boundary conditions and different angles of the edge of the planes, and concluded that the higher the planes wave angles, the less heterogeneous flow effects are and the heat transfer coefficients increase. They claimed that the corrugated heat exchangers increase the heat transfer, efficiency, and pressure drop in comparison with straight plane heat exchangers. Liu and Niu [21] investigated the effects of shape and angle on the flow regime and heat transfer in a corrugated channel.

Their results showed that the wave angle has a great effect on heat transfer and pressure drop. Boonloi and et. al. [22] investigated the turbulent forced convection in a corrugated channel with 30 and 45 degrees angles of attack for different Reynolds numbers, and showed an increase in heat transfer through the use of a corrugated channel and an increase in frictional losses. Recently, Omidi et.al. [23] reviewed the development methods of double-pipe heat exchangers, including active, passive and compound methods, and presented correlations of Nusselt number and pressure drop coefficient. With a review of the papers, it's obvious that none of them has considered the effects of external field, including magnetic field, on heat transfer. In their paper, the magnetic field is investigated only at a single point, and the flow is also investigated in a two dimension in low Reynolds number ranges.

According to the lack of study in the mentioned field, in the present paper, fluid flow and heat transfer are investigated in a triangular corrugated channel using OpenFOAM software.

Also, heat transfer in the presence of magnetic field at three different points including the initial, middle and the end of the channel in different Reynolds numbers has been investigated in order to achieve the optimal point for applying the magnetic field.

GOVERNING EQUATION

Fluid flow is described by mass conservation equations (continuity equation), momentum (Navier-Stokes) and energy equation (temperature equation for fluid). In a turbulent flow, the velocity and temperature values are divided into two values of mean and fluctuation, i.e. $u_j = U_j + u_j'$ and $= T + T'$.

These, together with the boundary conditions, form the following steady equations for the incompressible flow [4]:

$$\frac{\partial(\rho U_j)}{\partial x_j} = 0 \tag{1}$$

$$\frac{\partial}{\partial x_j}\left(\rho U_i U_j\right) = -\frac{\partial p}{\partial x_i} + \frac{\partial}{\partial x_j}(\tau_{ij} + \tau_{ij}^t) \tag{2}$$

$$\tau_{ij} = \mu\left(\frac{\partial U_i}{\partial x_j} + \frac{\partial U_j}{\partial x_i}\right); \tau_{ij}^t = -\rho\overline{u_i' u_j'} \tag{3}$$

$$\frac{\partial}{\partial x_j}(\rho c_p U_j T) = \frac{\partial}{\partial x_j}(q_j + q_j^t) \tag{4}$$

$$q_j = \frac{\mu c_p}{Pr}\frac{\partial T}{\partial x_j};\ q_j^t = -\rho c_p \overline{u_j' T'} \tag{5}$$

Where μ is the molecular viscosity ($kgm^{-1}s^{-1}$). Solving these equations is not analytically possible due to the nonlinear nature of the equations and the stochastic nature of the fluctuations. Turbulence stresses are calculated using following linear Eddy viscosity model. The shear stress in equation 3 is calculated as follows:

$$\tau_{ij}^t = \mu_t\left(\frac{\partial U_i}{\partial x_j} + \frac{\partial U_j}{\partial x_i}\right) - \frac{2}{3}\delta_{ij} k\rho \tag{6}$$

Where δ_{ij} is the Kronecker Delta function and when i = j , $\delta_{ij} = 1$ and when i ≠ j delta function is zero.

Many turbulence models have been proposed over the past few years. The k-ω model is the most famous two equation model. Unfortunately, it has been shown that the standard k-ε model is not suitable for predicting turbulent flow in corrugated geometry in transient flow regime. Instead, in the survey k-ω model has been used. Unlike the k-ε model, it is easier to determine boundary conditions in k-ω model. We know that in the solid boundary, k=0, and ω at some points of the primary mesh, away from the wall in obtained using $\omega = \frac{6\mu}{\beta y^2}$ (that y is the distance from the wall). Equations for obtaining k, ω and ν_t are as follows:
The macroscopic fluid densities and velocities are computed as below:

$$\nu_t = \frac{\mu_t}{\rho} = \frac{\alpha^* k}{\omega} \tag{7}$$

Kinetic energy k and specific dissipation rate ω equations are as follows:

$$U_j\frac{\partial k}{\partial x_j} = \tau_{ij}\frac{\partial U_i}{\partial x_j} - \beta^*\omega k + \frac{\partial}{\partial x_j}\left[(\nu + \sigma_k\nu_t)\frac{\partial k}{\partial x_j}\right] \tag{8}$$

$$U_j\frac{\partial \omega}{\partial x_j} = \frac{\sigma}{\nu_t}\tau\frac{\partial U_i}{\partial x_j} - \beta_2\omega^2 + \frac{\partial}{\partial x_j}\left[(\nu + \sigma_\omega\nu_t)\frac{\partial \omega}{\partial x_j}\right] + 2\sigma_{\omega 2}\frac{1}{\omega}\times\frac{\partial k}{\partial x_j}\frac{\partial \omega}{\partial x_j} \tag{9}$$

The constant of the model are as follows:

$$\beta^* = \frac{9}{100}\frac{\frac{5}{18} + \left(\frac{Re_t}{R_\beta}\right)^4}{1 + \left(\frac{Re_t}{R_\beta}\right)^4} \tag{10}$$

$$\alpha^* = \frac{\alpha_0^* + \frac{Re_t}{R_k}}{1 + \frac{Re_t}{R_k}} \tag{11}$$

$$\alpha = \frac{5}{9}\frac{\alpha_0 + \frac{Re_t}{R_\omega}}{1 + \frac{Re_t}{R_\omega}}(\alpha^*)^{-1} \tag{12}$$

The Reynolds number for turbulence flow is obtained using the following equation:

$$Re_t = \frac{\rho k}{\mu\omega} \tag{13}$$

$$\beta_2 = 0.078\frac{1 + \chi_\omega}{1 + 100\chi_\omega} \tag{14}$$

$$\chi_\omega = \left|\frac{\Omega_{ij}\Omega_{jk}\Omega_{ki}}{(0.09\omega)^3}\right| \tag{15}$$

$$\Omega_{ij} = \frac{1}{2}\left(\frac{\partial U_i}{\partial x_j} - \frac{\partial U_j}{\partial x_i}\right) \tag{16}$$

$$S_{ij} = \frac{1}{2}\left(\frac{\partial U_i}{\partial x_j} + \frac{\partial U_j}{\partial x_i}\right) \tag{17}$$

Other constants are:

$$\beta = 0.075, \alpha_0 = 0.1, \sigma_k = 0.5, \sigma_\omega = 0.5, R_\beta = 8,$$
$$R_k = 6, \alpha_0^* = \frac{\beta}{3}, R_\omega = 2.7, \sigma = 0.52, \sigma_{\omega 2} = 0.75$$

The term of turbulent heat transfer in equation 5 is determined by the following equation:

$$q^t = \frac{\mu_t}{\sigma_\theta}\frac{\partial T}{\partial x_j} \tag{18}$$

As stated, in this simulation an external magnetic field is used. The behavior of a bio-magnetic fluid is introduced under the influence of a magnetic field with magnetization property (M). Magnetic property means how much a magnetic field can affect the flow field. In equilibrium, the magnetic property is usually referred to as a relationship dependent on temperature and magnetic field density [24]:

$$M = K(T_c - T) \tag{19}$$

In which K is known as pyromagnetic coefficient and T_c as curie temperature. At temperatures higher than curie temperature, bio-magnetic fluid will not be exposed to the magnetic field. With considering little temperature variations [25], the following equation is considered for a constant temperature condition for magnetization property, which has a very high accuracy:

$$M = \chi_f H \tag{20}$$

Which χ_f is called the Ferro-fluid Magnetic susceptibility. For simulation of the magnetic field in OpenFOAM, the ideal wire carrying electric current equations are used. If the location of the conductive wire move particles in the desired location, in the perpendicular plane of the current carrying wire, the magnetic field is variable, and by moving away from the wire, the magnetic field strength decreases. With considering little temperature variations under the influence of the magnetic field, the continuity and momentum equations of the fluids are as follows:

$$\frac{\partial u}{\partial x} + \frac{\partial v}{\partial y} + \frac{\partial w}{\partial z} = 0 \tag{21}$$

$$u\frac{\partial u}{\partial x} + v\frac{\partial u}{\partial y} + w\frac{\partial u}{\partial z} = -\frac{1}{\rho}\frac{\partial P}{\partial x} + \nu\left(\frac{\partial^2 u}{\partial x^2} + \frac{\partial^2 u}{\partial y^2} + \frac{\partial^2 u}{\partial z^2}\right) + \frac{\mu_0 M}{\rho}\frac{\partial H}{\partial x} \tag{22}$$

$$u\frac{\partial v}{\partial x} + v\frac{\partial v}{\partial y} + w\frac{\partial v}{\partial z} = -\frac{1}{\rho}\frac{\partial P}{\partial y} + \nu\left(\frac{\partial^2 v}{\partial x^2} + \frac{\partial^2 v}{\partial y^2} + \frac{\partial^2 v}{\partial z^2}\right) + \frac{\mu_0 M}{\rho}\frac{\partial H}{\partial y} \tag{23}$$

$$u\frac{\partial w}{\partial x} + v\frac{\partial w}{\partial y} + w\frac{\partial w}{\partial z} = -\frac{1}{\rho}\frac{\partial P}{\partial z} + \nu\left(\frac{\partial^2 w}{\partial x^2} + \frac{\partial^2 w}{\partial y^2} + \frac{\partial^2 w}{\partial z^2}\right) + \frac{\mu_0 M}{\rho}\frac{\partial H}{\partial z} \tag{24}$$

In this relations ν is the kinematic viscosity and $B = \mu_0 H$ is called the induction of the magnetic field. Assuming the magnetic field strength changes in the x-y plane, the electromagnetic force applies to the fluid in these two directions, and since the field changes along z are zero, the magnetic force in this direction is zero. The magnitude of the magnetic field intensity H_x and H_y along the x and y around the electric conductor wire is considered as follows:

$$H_x = \frac{\gamma}{2\pi}\frac{x - a}{(x - a)^2 - (y - b)^2} \tag{25}$$

$$H_x = -\frac{\gamma}{2\pi}\frac{y - b}{(x - a)^2 - (y - b)^2} \tag{26}$$

Where a and b are the locations of the conductive wire and γ is the strength of the magnetic field at this point. The magnitude of the magnetic field strength at any point is obtained by the following equation. The magnetic field variations are on the x-y plane, so the terms $\frac{\mu_0 M}{\rho}\frac{\partial H}{\partial x}$ and $\frac{\mu_0 M}{\rho}\frac{\partial H}{\partial y}$ show the effective forces on the fluid momentum along x and y direction and the field density is obtained from the following equation:

$$H_{(x,y)} = \sqrt{H_x^2 + H_y^2} = \frac{\gamma}{2\pi}\frac{1}{\sqrt{(x-a)^2 + (y-b)^2}} \qquad (27)$$

As mentioned, in this paper the magnetic field is applied at three points of the geometry, including initial, middle and end of the channel, as shown in Figure 1.

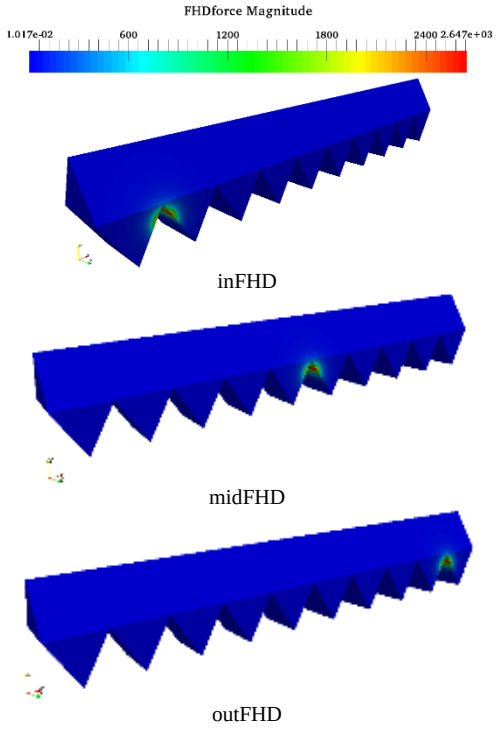

Fig. 1. Different locations of applying magnetic field

Mesh and boundary conditions

The length of the channel is 0.1 m and its hydraulic diameter is $D_h = 13mm$. Gambit software is used for meshing. Figure 2 shows a fully structured mesh generated for 2.5 cycles of the corrugated channel. The distance between the first adjacent cell from wall to consider y^+ is equal to 0.0001 m.

No-slip boundary condition is used for the walls. Two fixed heat fluxes of 530 and 1200 W/m^2 are applied to corrugated walls as thermal boundary conditions. At inlet, the uniform velocities of 1, 2, 3, 4, 5, and 6 m/s are applied to consider the effect of different Reynolds numbers. The input temperature is 25 °C and the outlet pressure is 1 atm. The turbulence intensity is also 5%.

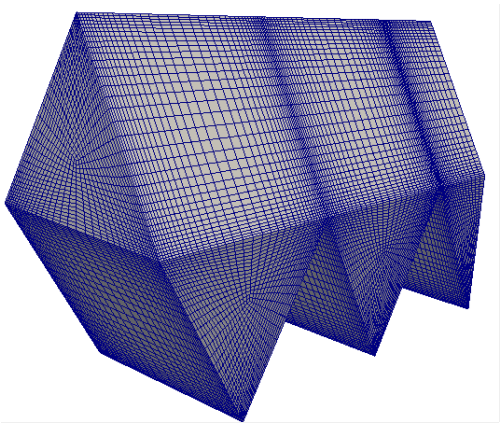

Fig. 2. Computational domain meshing

In order to verify the grid independency, three different number of elements are considered 405000, 699840 and 960000, and the difference between Nusselt number for these grid numbers is investigated.

As shown in Figure 3, the Nusselt numbers of the two smaller grids coincided exactly, so the final calculations are done with the mesh number of 699840.

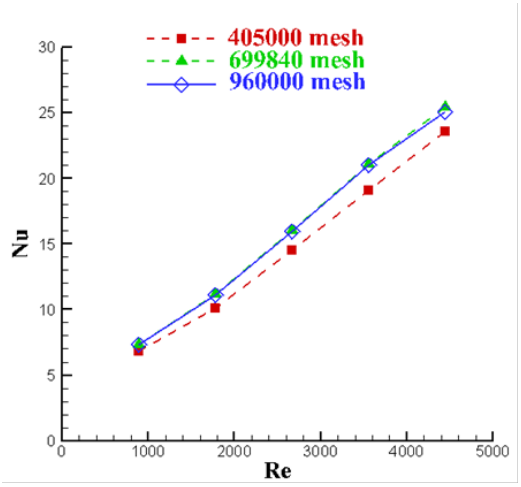

Fig. 3. Grid independency

VALIDATION

In order to validate the OpenFOAM solver, the experimental and numerical results in reference [4] are considered for validation of the average Nusselt number and the friction coefficient.

As shown in Figure 4, the OpenFOAM results are in good agreement with experimental data. The mean value of the error for the Nusselt number is 3.197% for the experimental data and for the friction coefficient is 12.137% compared to the experimental data.

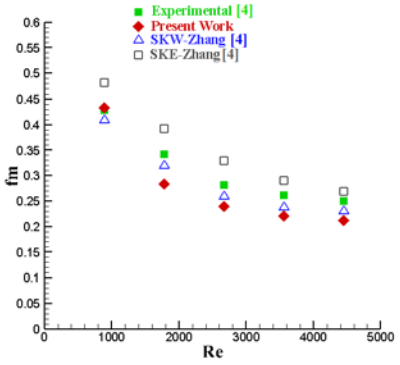

4a

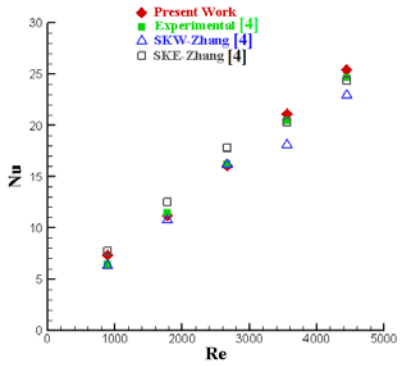

4b

Fig. 4. Validation; a) average Nusselt number b) friction coefficient

RESULTS AND DISCUSSION

In this paper, water is selected as the fluid. The velocity and temperature fields in the channel are calculated using k-ω model. by calculating the output temperature and pressure drop, Nusselt number and average friction coefficient could be calculated. The average Nusselt number is defined as follows:

$$Nu_m = \frac{h_m D_h}{\lambda} \tag{28}$$

Where λ is the water conductivity coefficient (W/m.K), D_h is the hydraulic diameter and h_m is the convection heat transfer coefficient which is obtained as follows:

$$h_m = \frac{E_p}{A_t \Delta T_{lg}} \tag{29}$$

Where A_t is the total surface area of the heat exchanger (m^2), E_p is the heating power (KW) and ΔT_{lg} is the logarithmic temperature difference between the wall and the fluid which is calculated as follows:

$$E_p = \dot{m}_v c_p (T_{fo} - T_{fi}) \tag{30}$$

$$\Delta T_{lg} = \frac{(T_{wi} - T_{fi}) - (T_{wo} - T_{fo})}{ln[(T_{wi} - T_{fi})/(T_{wo} - T_{fo})]} \tag{31}$$

Where $\dot{m}_v$ is the mass flow rate (kg/s), and c_p is the specific heat value (kJ/kg.K). f, w, i and o are fluid, wall, inlet and outlet respectively.
The Reynolds number is defined as follows:

$$Re = \frac{U_i D_h}{\nu} \tag{32}$$

The average Darcy friction factor is calculated as follows:

$$f_m = \frac{\frac{P_{fi} - P_{fo}}{L_t} D_h}{\frac{1}{2}\rho U_i^2} \tag{33}$$

Where L_t is the length of the channel (m), ρ is density (kg/m^3), P_{fi} and P_{fo} are pressure (Pa) at inlet and outlet of the channel respectively. Figure 5a and b, show a comparison between the average Nusselt values for the non-FHD state and the three different locations FHDs in the two thermal fluxes of 530 and 1200 W/m^2 respectively. As seen from this figure, the field applied at the initial part of the channel has the most Nusselt number than the rest locations of applying FHD. In all cases, the Nusselt number has increased with Reynolds's increase.

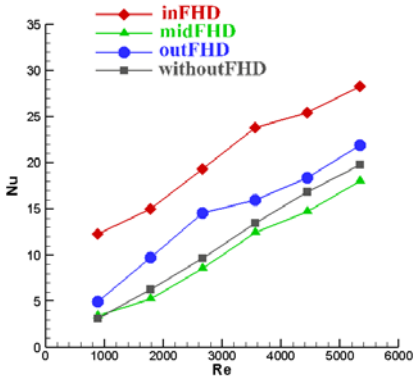

5a($q'' = 530 \frac{W}{m^2}$)

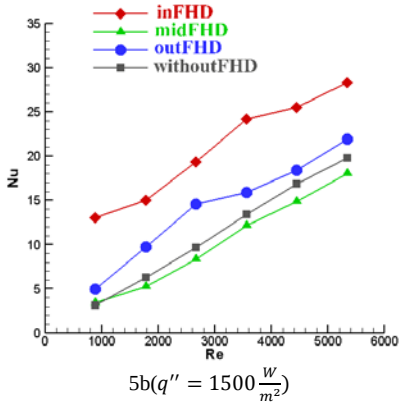

5b($q'' = 1500 \frac{W}{m^2}$)

Fig. 5. Average Nusselt number profile in respect to Reynolds number

Table 1 shows the Nusselt number change due to the application of the magnetic field to different regions in thermal flux of q" = 530 W/m^2 Nusselt variations follow the same trend for two thermal fluxes.

Table 1
Nusselt variation percentage.

Re	ΔNu_{inFHD}(%)	ΔNu_{midFHD}(%)	ΔNu_{outFHD}(%)
889.96	289.811	8.869	56.2711
1779.93	139.018	-15.766	54.5416
2669.89	100.145	-11.504	50.898
3559.85	77.348	-7.426	18.774
4449.82	51.019	-12.552	9.09766
5339.77	42.76	-9.0844	10.5533

Figure 6(a-d) shows the comparison between velocity contours for the non-FHD mode and three FHD application areas in the 530 W/m^2 thermal flux.

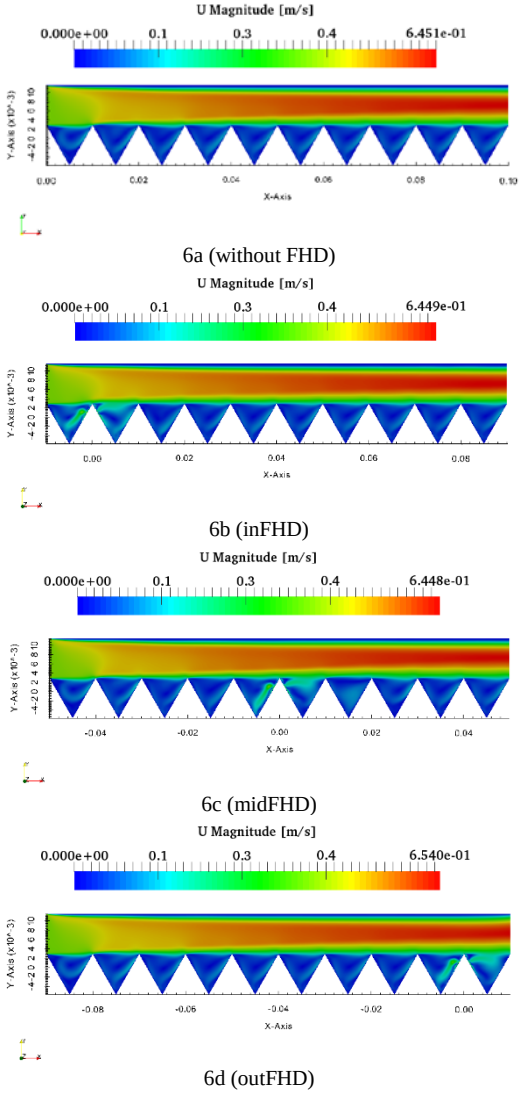

Fig. 6. Velocity contour comparison in $q" = 530\ W/m^2$

As shown in Figure 6a, the application of a magnetic field causes vortices in the duct valleys, resulting in an intensification of the momentum transfer and a better mixing of the flow, which improves overall heat transfer, as shown in Figure 5.

Figure 7(a-d) shows the comparison between the temperature contours for the non-FHD state and the three FHD application areas in the thermal flux of 530 W/m^2. The intensification of vortices by applying the magnetic field in each position leads to a decrease in the temperature in that position. The flow is heated up through the influence of a heat flux that enters from the lower corrugated wall. In Figure 7a, this heating is done without any external force, the application of the magnetic field at the initial part of the channel reduces the temperature in this area, thereby increasing the temperature difference between the inlet and the outlet, which increases the Nusselt number.

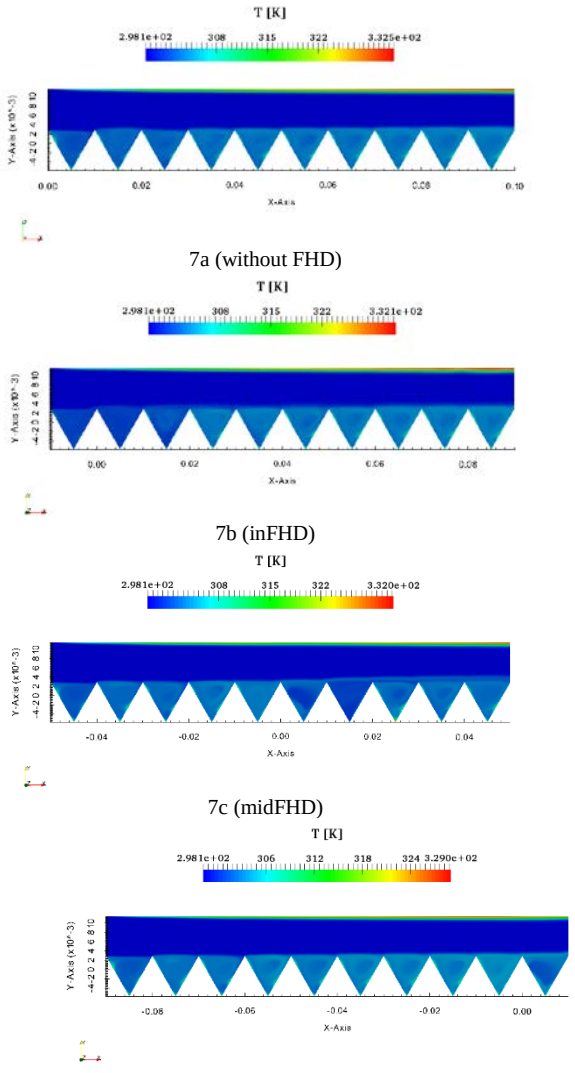

Fig. 7. Temperature contour comparison in $q" = 530\ W/m^2$

The application of a magnetic field in the middle part of the channel causes a sudden drop in the fluid that is being heated up, and the fluid should find time to re-heat. As a result, the difference between the input and output temperatures is reduced to the extent that it reduces the Nusselt number even less than the case with non-magnetic field. By applying the magnetic field at the end of the channel, the temperature difference in the bottom of the channel where the velocity is low increases slightly compared to the non-magnetic field case, which improves the heat transfer.

Figure 8a and b, show a comparison between the average Darcy friction coefficient for the non-FHD state and the three FHD application regions in two thermal fluxes of 530 and 1200 W/m^2 respectively. As can be seen from this figure, the applied field in the initial portion of the channel also has the lowest coefficient of friction than the rest of the states. In all cases, the friction coefficient decreases with increasing Reynolds number but increases for inFHD case.

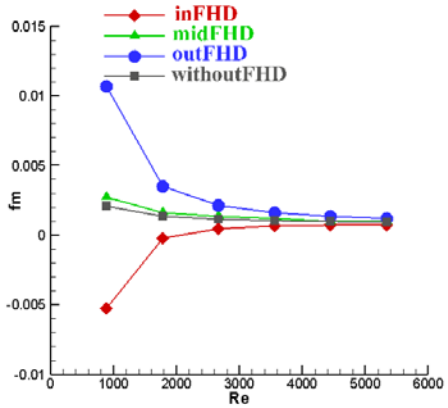

8a($q'' = 530 \frac{W}{m^2}$)

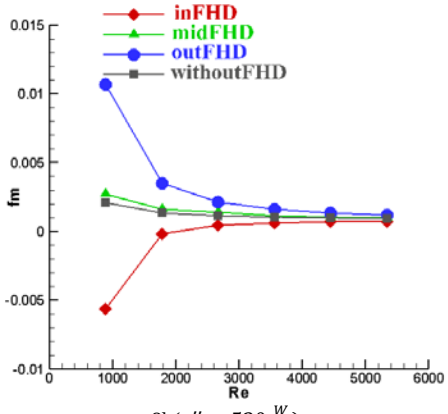

8b($q'' = 530 \frac{W}{m^2}$)

Fig. 8. Average friction factor in respect to Reynolds number

By applying field at the inlet and thereby increasing the vortex and momentum transfer, the difference in pressure between the inlet and the outlet is reduced, that reduces the friction coefficient in this case. The application of the magnetic field in the middle of the channel does not have much effect on the pressure difference in the inlet and outlet, and, as shown in Figure 8, there has not been much difference with the non- magnetic field case.

CONCLUSION

Fluid flow and convection heat transfer in a triangular corrugated channel under two constant heat fluxes and different Reynolds numbers have been investigated. A three-dimensional numerical study was conducted to analyze the effect of magnetic field in different regions. The k-ω model was used in low Reynolds numbers and was validated by numerical and experimental results [4]. For the investigated Reynolds range, the results are as follows:

- Nusselt number increases with increasing Reynolds number in all situations of magnetic field application.
- The friction coefficient increases with the increase of Reynolds number only in the case of inFHD. But its value is still lower than applying the field on other areas.
- According to the investigations, the optimal area of application of the magnetic field is at the channel entrance region, which increases the Nusselt number and decreases the coefficient of friction.

REFERENCES

[1] Sawyers DR, Sen M, Chang HC. Heat transfer enhancement in three-dimensional corrugated channel flow. International journal of heat and mass transfer. 1998 Nov 1;41(22):3559-73.

[2] Zhang LZ. Numerical study of periodically fully developed flow and heat transfer in cross-corrugated triangular channels in transitional flow regime. Numerical Heat Transfer, Part A: Applications. 2005 Sep 1;48(4):387-405.

[3] Naphon P. Effect of wavy plate geometry configurations on the temperature and flow distributions. International Communications in Heat and Mass Transfer. 2009 Nov 1;36(9):942-6.

[4] Zhang LZ, Chen ZY. Convective heat transfer in cross-corrugated triangular ducts under uniform heat flux boundary conditions. International Journal of Heat and Mass Transfer. 2011 Jan 15;54(1-3):597-605.

[5] Yin J, Yang G, Hao G, Lv P. Numerical Investigation of Flow and Heat Transfer in Corrugated Sinusoidal Wavy Channel. InPower and Energy Engineering Conference (APPEEC), 2011 Asia-Pacific 2011 Mar 25 (pp. 1-5). IEEE.

[6] Ramiar A, Ranjbar AA, Hosseinizadeh SF. Effect of axial conduction and variable properties on two-dimensional conjugate heat transfer of Al_2O_3-eg/water mixture nanofluid in microchannel.

[7] Nourani Zonouz O, Salmanpour M. Numerical Analysis of Flow Field and Heat Transfer of 2D

Wavy Ducts and Optimization by Entropy Generation Minimization Method. Journal of Thermodynamics. 2012 Feb 9;2012.

[8] Al-Jabair S. Comparison between RANS and LES fo Turbulence Models in CFD Simulation Using OpenFOAM.

[9] Ramgadia AG, Saha AK. Numerical study of fully developed flow and heat transfer in a wavy passage. International Journal of Thermal Sciences. 2013 May 1;67:152-66.

[10] Midhun P, Rahul H Kumar, K.S Santhosh. Numerical simulation of flow through mini channels with internal obstructions. International Journal of Innovative Research in Science, Engineering and Technology. 2013 Dec 2;1:800-809.

[11] Ramgadia AG, Saha AK. Three-dimensional numerical study of turbulent flow and heat transfer in a wavy-walled duct. International Journal of Heat and Mass Transfer. 2013 Dec 1;67:98-117.

[12] Benchabi R, Lanani A. Forced Convection of the Bi and Three-Dimensional Flow in a Periodic Channel. Journal of Materials Science and Engineering. B. 2013 Oct 1;3(10B).

[13] Deylami HM, SANAEI M, KOUHI KR. Numerical investigation of heat transfer and pressure drop in a corrugated channel.

[14] Khoshvaght-Aliabadi M. Influence of different design parameters and Al_2O_3-water nanofluid flow on heat transfer and flow characteristics of sinusoidal-corrugated channels. Energy conversion and management. 2014 Dec 1;88:96-105.

[15] Ahmed MA, Yusoff MZ, Ng KC, Shuaib NH. The effects of wavy-wall phase shift on thermal-hydraulic performance of Al2O3–water nanofluid flow in sinusoidal-wavy channel. Case Studies in Thermal Engineering. 2014 Nov 1;4:153-65.

[16] Ahmed MA, Yusoff MZ, Ng KC, Shuaib NH. Numerical and experimental investigations on the heat transfer enhancement in corrugated channels using SiO_2–water nanofluid. Case Studies in Thermal Engineering. 2015 Sep 1;6:77-92.

[17] Mirzaei M, Sohankar A, Davidson L, Innings F. Large Eddy Simulation of the flow and heat transfer in a half-corrugated channel with various wave amplitudes. International Journal of Heat and Mass Transfer. 2014 Sep 1;76:432-46.

[18] Naghibi MF, Rahimi-Esbo M, Mohammadyari R, Mobini K. Investigation of flow and heat transfer of nanofluid in a diverging sinusoidal channel. International Journal of Nano Dimension. 2015 Jul 1;6(3):241.

[19] Gao X, Li W, Wang J. Heat transfer and flow characteristics in a channel with one corrugated wall. Science China Technological Sciences. 2014 Nov 1;57(11):2177-89.

[20] Li ZX, Zhong TS, Niu JL, Xiao F, Zhang LZ. Conjugate heat and mass transfer in a total heat exchanger with cross-corrugated triangular ducts and one-step made asymmetric membranes. International Journal of Heat and Mass Transfer. 2015 May 1;84:390-400.

[21] X. P. Liu, J. L. Niu: Effects of geometrical parameters on the thermohydraulic characteristics of periodic cross-corrugated channels, International Journal of Heat and Mass Transfer, 84 (2015) 542-549.

[22] Boonloi A, Jedsadaratanachai W. Turbulent forced convection in a heat exchanger square channel with wavy-ribs vortex generator. Chinese Journal of Chemical Engineering. 2015 Aug 1;23(8):1256-65.

[23] Omidi M, Farhadi M, Jafari M. A comprehensive review on double pipe heat exchangers. Applied Thermal Engineering. 2017 Jan 5;110:1075-90.

[24] Andersson HI, Valnes OA. Flow of a heated ferrofluid over a stretching sheet in the presence of a magnetic dipole. Acta Mechanica. 1998 Mar 1;128(1-2):39-47.

[25] Tzirtzilakis1 EE, Sakalis VD, Kafoussias NG, Hatzikonstantinou PM. Biomagnetic fluid flow in a 3D rectangular duct. International Journal for Numerical Methods in Fluids. 2004 Apr 30;44(12):1279-98.